Japanese Journal of Applied Physics

The Japan Society of Applied Physics

REGULAR PAPER • OPEN ACCESS

Microscopic analysis of interface composition dynamics in m-plane AlInN

OPEN ACCESS

Japanese Journal of Applied Physics **58**, SC1008 (2019) **REGULAR PAPER**

https://doi.org/**10.7567/1347-4065/ab079d**

Microscopic analysis of interface composition dynamics in m-plane AlInN

Philipp Horenburg[1*], Heiko Bremers[1,2], Robert Imlau[3], Uwe Rossow[1], and Andreas Hangleiter[1,2]

[1]*Institute of Applied Physics, Technische Universität Braunschweig, Mendelssohnstraße 2, 38106 Braunschweig, Germany*
[2]*Laboratory for Emerging Nanometrology, Braunschweig, Germany*
[3]*Thermo Fisher Scientific, Achtseweg Noord 5, 5651 GG Eindhoven, The Netherlands*

[*]E-mail: p.horenburg@tu-braunschweig.de

Received November 8, 2018; accepted January 18, 2019; published online April 17, 2019

We present first microscopic evidence on approximately two monolayers of interfacial indium depletion in one-directionally lattice-matched AlInN grown on m-plane GaN as measured by energy dispersive X-ray spectroscopy. Contrary to other reports, we find no significant incorporation of parasitic gallium into the volume material, but only some spreading of gallium across the GaN/AlInN heterointerface. Using a quantitative description of this behaviour, we conclude that the observed effects are not depending on the crystal orientation, nominal stoichiometry and strain state of the AlInN, but rather represent an inherent characteristic of its growth dynamics, related to the differences in metal-nitrogen binding energies of AlN and InN. © 2019 The Japan Society of Applied Physics

1. Introduction

While the ternary group-III nitride alloys GaInN and AlGaN have intensively been studied, the field of AlInN as the third remaining member of this family remains rather undiscovered. This is not least owed to the circumstance that this material has a rather small window of suitable growth conditions in metal organic vapor phase epitaxy (MOVPE) and due to the large discrepancy in lattice constants of its binary constituents AlN ($a = 3.111\,97$ Å[1]) and InN ($a = 3.537\,74$ Å[2]). On the other hand, unlike the two first-mentioned alloys, AlInN can be grown lattice-matched to GaN in various crystal orientations[3] by controlling the composition according to Vegard's law.[4,5] When grown lattice-matched along the *a*-axis of GaN, AlInN has a higher contrast in refractive indices to GaN compared to AlGaN,[6,7] making it a promising choice for application in distributed Bragg-reflectors[6] and cladding layers.[8,9]

However, epitaxial growth of AlInN of high crystalline quality remains a challenging endeavour, struggling with intrinsic degradation of the crystal quality[10,11] and phase separation,[12–15] especially for thick layers and high indium concentrations.[16] Reference 17 observed a dependence of the indium concentration of AlInN on its layer thickness in c-plane AlInN/GaN superlattice structures and concluded the formation of an approximately 0.4 nm thick layer of pure AlN during the initial stage of growth. Moreover, as another impact on the composition, parasitic auto-incorporation of up to 45% of gallium into bulk Al(Ga)InN due to diffusion from GaN templates[18] and reactor sidewalls[19–23] has been reported. Further, AlInN has been demonstrated to act as a strain manipulating buffer layer in nonpolar multi quantum well structures, significantly increasing the indium incorporation into GaInN quantum wells.[24] Beyond that, efficient radiative recombination has been shown in m-plane AlInN over a wide spectral range. Therefore, its growth behaviour in nonbasal orientations is of particular interest.[25,26] We present a quantitative microscopic analysis of the interface composition of nonpolar m-plane AlInN grown on GaN.

2. Experimental details

Our studies were carried out on a sample grown via low pressure MOVPE in a commercial AIXTRON AIX200RF system. The structure consists of a pseudo-bulk m-plane GaN substrate, overgrown with an epitaxial GaN buffer layer, 130 nm AlInN and a five-fold GaInN/GaN multi quantum well structure. We use common group-III precursors TMAl, TEGa/TMGa and TMIn for aluminum, gallium and indium supply, respectively. Ammonia serves as the nitrogen source and the carrier gases are N_2 for AlInN and H_2 for GaN template growth. All layers containing indium were grown in the indium supersaturated regime, i.e. the composition is primarily controlled by the process temperature. The AlInN is grown at a total pressure of 20 mbar with V/III ratio of approximately 1800. The growth temperature was set to 800 °C, corresponding to a nominal indium concentration of 28% for lattice matching along the *c*-axis of the GaN growth template. In epitaxy of nonpolar m-plane structures, the crystallographic in-plane directions are the *a*- and *c*-axes. Since group-III nitrides have different a/c-ratios, the resulting strain state is anisotropic. Thus, only one-directional lattice matching can be achieved. In this case, this leads to compressive strain along the *a*-axis. Here, the AlInN buffer layer is utilized for strain manipulation of the top grown multi quantum well. A detailed analysis of the strain state, structural and optical properties of this structure, especially of the AlInN and the MQW, has been published elsewhere.[24]

The sample has undergone an extensive high-resolution X-ray diffraction (HRXRD) analysis[24] using a Panalytical X'Pert Pro system. In order to determine the composition, in- and out-of-plane lattice constants and to assess the strain state, on- and off-axis reciprocal space maps as well as relative scans of several reflections have been measured. The actual indium composition of the AlInN has been determined to be approximately 29%, close to the c-lattice-matching condition. Based on the HRXRD analysis, the occurrence of phase separation, as described for thick c-plane AlInN layers,[12–14] can be excluded. For a microscopic analysis of the lower GaN/AlInN interface, scanning transmission

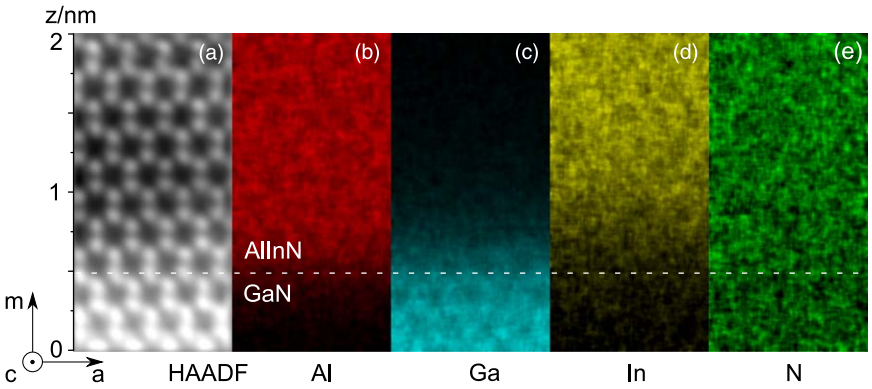

Fig. 1. (Color online) HAADF (a) and EDS measurements of aluminum (b), gallium (c), indium (d) and N (e) across the GaN/AlInN interface (dashed horizontal line) in projection of the crystallographic *c*-axis.

electron microscopy (STEM) has been carried out for high-angle annular dark field (HAADF) measurements and energy dispersive X-ray spectroscopy (EDS) in a FEI Titan Themis[3] 300. The investigations were done using a C_S-corrected setup at an acceleration voltage of 200 kV. The combination of these modes enables imaging with atomic resolution (HAADF) as well as compositional analysis (EDS) with nearly atomic resolution. The preparation of the lamella was done using focused ion beam milling.

3. Results and discussion

Figure 1 depicts the HAADF image [Fig. 1(a)] and element-specific EDS maps [Figs. 1(b)–1(d)] of the GaN/AlInN interface. Since the crystallographic c-direction is the axis of projection, the hexagonal basal plane is clearly visible in the HAADF image, illustrating the structural integrity of the heterointerface and demonstrating the high quality of both the sample and the STEM imaging. There are no visible defects within the region of analysis. The EDS maps [Fig. 1(b) to Fig. 1(d)] contain no direct structural information, but are sensitive to the different atomic species. The color gradients in the EDS maps of Ga, aluminum and indium indicate the compositional transition from GaN to AlInN at a constant level of N [Fig. 1(e)]. Comparing the aluminum [Fig. 1(b)] and the indium [Fig. 1(d)] composition gradient, the indium profile appears slightly broader with its nominal concentration achieved at later instant during the growth process.

For a more quantitative analysis, integrated line scans across the heterointerface along the growth direction have been carried out for the EDS map of each group-III element (Fig. 2). The origin in Fig. 2 relates to the lower end of the images depicted in Figs. 1(b)–1(d) and does not mark the actual interface. First, the Al profile has the sharpest transition and serves as a lower estimation for the spatial resolution of the instrument. Further, it becomes obvious that no gallium is incorporated into the bulk AlInN. Even though there is some spread of gallium atoms across the heterointerface, the profile drops towards zero with increasing layer thickness. Moreover, while the aluminum composition reaches a constant value after approximately 1 nm of grown material, the slope of the indium profile does not vanish until about 1.5 nm of layer thickness.

According to Vegard's rule[5)] and expecting a quarternary material at the heterointerface, the m-lattice constant along the growth direction can be written as

$$m(z) = \sqrt{3}\,\{x(z)\cdot a_{\mathrm{AlN}} + y(z)\cdot a_{\mathrm{GaN}} + u(z)\cdot a_{\mathrm{InN}}\} \quad (1)$$

with the Al, Ga and In compositions $x(z)$, $y(z)$ and $u(z)$, respectively. The amount of atoms in the group-III sublattice is conserved, i.e.:

$$u(z) + x(z) + y(z) = 1. \quad (2)$$

Assuming the probability density of incorporating an atom at a given site to be Gaussian, the concentration profiles can be reproduced using error functions of width w_{Al}, centered at z_{Al}, z_{In}, i.e. by taking the example of aluminum:

$$x(z) = \frac{1}{2}x_{\mathrm{bulk}}\left[1 + \mathrm{erf}\left(\frac{z - z_{\mathrm{Al}}}{w_{\mathrm{Al}}}\right)\right]. \quad (3)$$

The bulk concentration $x_{\mathrm{bulk}} = 0.71$ is measured by HR-XRD. With $x(z)$ and $u(z)$, the Ga concentration $y(z)$ can be calculated using Eq. (2). The measured signal is periodically modulated, reflecting the crystal periodicity. This can easily accounted for by superimposing the transition profiles with an harmonic oscillation. Further, a background intensity has to be considered, accounting for the dark count rate in the experiment. The crucial fit parameters are listed in Table I.

The width w of the transition is almost twice as large for indium as compared to aluminum. Thus, the incorporation of aluminum into the group-III sublattice stabilizes faster in the growth process as compared indium, the latter of which shows a broadened transition. Besides the sharpness of the transition, the center of the interface is also shifted by approximately 0.35 nm. Moreover, there is hardly any gallium incorporated into the bulk AlInN. However, the distribution of Ga atoms suggests that in the initial stage of AlInN growth, Ga tends to replace the indium in the group-III sublattice. This raises the question to what extent the incorporation dynamics of Ga and In are connected to each other.

As long as TMGa is supplied in the gas phase during the GaN growth, the source of gallium atoms is virtually infinite. However, when the TMGa supply is stopped, the gallium source becomes exhaustible and is given by the amount of gallium atoms in the adlayer[27,28)] covering the growth surface. After the growth of GaN, the reactor temperature is ramped down from 1180 °C to 800 °C for subsequent AlInN growth. During this time, there is no gas supply of group-III precursors, whereas the ammonia supply remains constant. With decreased thermal energy, the desorption of

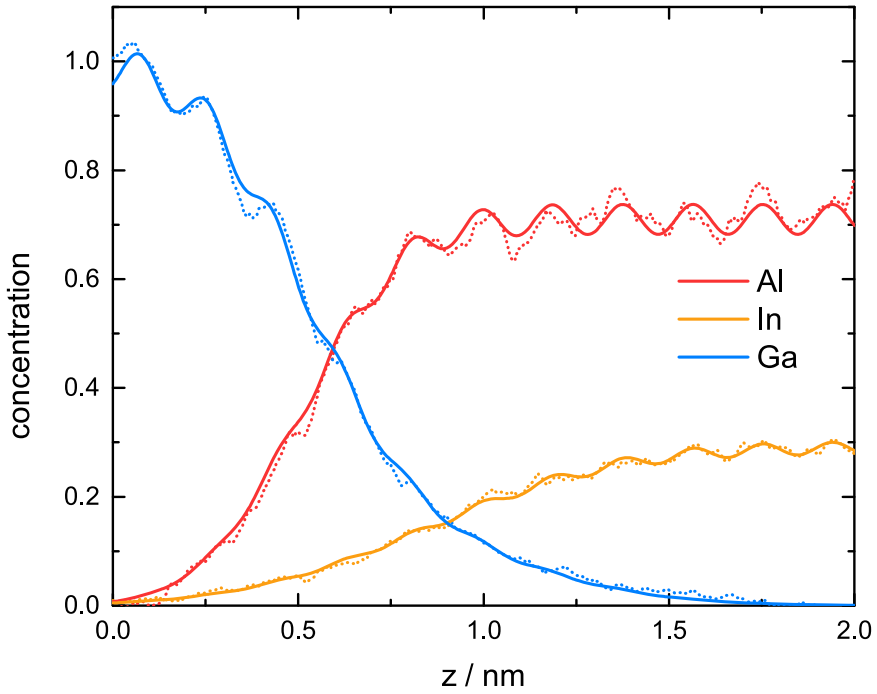

Fig. 2. (Color online) Concentration profiles derived from the EDS maps shown in Fig. 1 in combination with the composition as measured by HR-XRD. The measured data are plotted in dotted lines, the applied fit functions (see text) are shown with solid lines. The abscissa relates to the crystallographic growth direction (*m*-axis).

Table I. Essential fit parameters to describe the profiles depicted in Fig. 2.

Parameter	Al	In
w nm^{-1}	0.311	0.573
z nm^{-1}	0.508	0.855

gallium from the adlayer is reduced, which can be understood as a stabilizing effect on gallium in the adlayer, prolonging its exhaustion. Further, with beginning supply of TMIn and TMAl, two new atomic species are introduced, constituting practically endless sources of group-III atoms and influencing the composition of the adlayer. Under these new conditions, the incorporation of the remaining gallium competes with the other metal species. Among these, the indium atoms are the most weakly bond species with an binding energy of 1.93 eV.[30] Hence, desorption is the dominant mechanism of indium removal from the surface,[29] whereas its incorporation is rather inefficient. Al, however, is strongly bound to the growth surface (binding energy of 2.88 eV[30]) and therefore far from its desorption limit. Thus, more energy is gained by binding aluminum atoms to the surface instead of indium. This is reflected by both w and z for aluminum and indium (see Table I). Judging from this, exhaustion of the remaining gallium atoms in the adlayer is mainly delayed by the fast onset of aluminum incorporation. On the other hand, in the presence of remaining Ga, the efficient incorporation of indium is prevented. As the gallium source comes close to exhaustion, indium incorporation gradually becomes more efficient, leading to a slow decay of the gallium concentration. In this process, the composition of the adlayer covering the growth surface gradually changes its composition from Ga-rich to In-rich. Further, considering the surface energy, the growth mode is expected to be rather three dimensional due to the low surface mobility of aluminum atoms. Thus, the formation of AlN islands accumulates strain energy with increasing layer thickness. Again, the incorporation of indium atoms becomes more probable as the Al(In)N layer thickness increases, reducing the overall strain energy.

From these observations, we conclude the formation of an In-depleted phase at the initial stage of m-plane AlInN growth. The thickness of this depletion region is given by the difference of the transitions centers $\Delta z = z_{\mathrm{In}} - z_{\mathrm{Al}} \approx 3.5$ Å as extracted from the fits of the EDS profiles of aluminum and indium. Since the same behaviour has been reported by Ref. 17 with an In-depleted phase of about 3.9 Å thickness in lattice-matched c-plane AlInN/GaN super lattice structures, we further conclude that this effect is independent of the crystal orientation, nominal composition and strain state, but instead is inherent to the growth dynamics of GaN/AlInN interfaces. This clearly distinguishes the indium incorporation dynamics of AlInN from GaInN, where dependencies on the crystal orientation have been discussed.[31] We further see small amounts of gallium being carried over the interface, but no significant gallium incorporation into the volume of the AlInN as reported in the literature.[18–23] Under the given growth conditions, the fraction of gallium spread across the interface is substantially lower than the amount of parasitically incorporated gallium reported elsewhere.[18] This indicates the presence of an exhaustible source of gallium atoms, most probably in terms of a gallium adlayer from the preceding GaN growth. As the indium supplied by the gas atmosphere is much closer to its desorption limit compared to the Ga, the incorporation of gallium atoms is preferred among both species. In this scenario, stable conditions for an efficient indium uptake are reached when the remaining gallium is fully incorporated.

4. Summary

In conclusion, the heterointerface of m-plane $Al_{0.71}In_{0.29}N$ one-directionally lattice-matched to GaN has been investigated by STEM in HAADF and EDS mode. Whereas the crystal

structure is intact within the region of analysis, line scans across the interface reveal the formation of an ≈3.5 Å thick In-depleted phase before stable AlInN growth is established. Beyond that, the profile of the gallium group-III sublattice suggests small fractions of gallium being spread across the heterointerface with no parasitic incorporation into the bulk AlInN. Especially for thin AlInN films, these observations indicate significant deviations from the nominal composition under the given growth conditions.

1) W. Paszkowicz, S. Podsiadło, and R. Minikayev, J. Alloys Compd. **382**, 100 (2004).
2) W. Paszkowicz, R. Černý, and S. Krukowski, Powder Diffr. **18**, 114 (2004).
3) E. R. Buß, P. Horenburg, U. Rossow, H. Bremers, T. Meisch, M. Caliebe, F. Scholz, and A. Hangleiter, Phys. Status Solidi B **253**, 84 (2015).
4) H. M. Foronda, B. Mazumder, E. C. Young, E. C. Young, M. A. Laurent, Y. Li, S. P. DenBaars, and J. S. Speck, J. Cryst. Growth **475**, 127 (2017).
5) L. Vegard, Z. Phys. **5**, 17 (1921).
6) J. F. Carlin, J. Dorsaz, C. Zellweger, S. Gradecak, and M. Ilegems, 2003 International Symposium on Compound Semiconductors: Post-Conference Proceedings, 2003, p. 36.
7) J. F. Carlin, C. Zellweger, J. Dorsaz, S. Nicolay, G. Christmann, E. Feltin, R. Butté, and N. Grandjean, Phys. Status Solidi C **8**, 2326 (2005).
8) R. Charash, H. Kim-Chauveau, A. Vajpeyi, M. Akther, P. P. Maaskant, E. Frayssinet, P. De Mierry, J.-Y. Duboz, and B. Corbett, Phys. Status Solidi C **8**, 2378 (2008).
9) A. Castiglia, E. Feltin, J. Dorsaz, G. Cosendey, J.-F. Carlin, R. Butté, and N. Grandjean, Electron. Lett. **44**, 8 (2011).
10) G. Perillat-Merceroz, G. Cosendey, J.-F. Carlin, R. Butté, and N. Grandjean, J. Appl. Phys. **113**, 063506 (2013).
11) Z. T. Chen, K. Fujita, J. Ichikawa, and T. Egawa, J. Appl. Phys. **111**, 053535 (2012).
12) Q. Y. Wei, T. Li, Y. Huang, J. Y. Huang, Z. T. Chen, T. Egawa, and F. A. Ponce, Appl. Phys. Lett. **100**, 092101 (2012).
13) A. Minj, D. Cavalcoli, and A. Cavallini, Appl. Phys. Lett. **97**, 132114 (2010).
14) A. Redondo-Cubero, K. Lorenz, R. Gago, N. Franco, M.-A. di Forte Poisson, E. Alvers, and E. Muñoz, J. Phys. D: Appl. Phys. **43**, 055406 (2010).
15) C. Hums, J. Bläsing, A. Dadgar, A. Diez, T. Hempel, J. Christen, A. Krost, K. Lorenz, and E. Alves, Appl. Phys. Lett. **90**, 022105 (2007).
16) T. Kajima, A. Kobayashi, K. Ueno, J. Ohta, H. Fujioka, and M. Oshima, Appl. Phys. Express **6**, 021003 (2013).
17) R. Buß, U. Rossow, H. Bremers, and A. Hangleiter, Appl. Phys. Lett. **104**, 162104 (2014).
18) J. J. Zhu et al., J. Cryst. Growth **348**, 25 (2012).
19) M. Hiroki, Y. Oda, N. Watanabe, N. Maeda, H. Yokoyama, K. Kumakura, and H. Yamamoto, J. Cryst. Growth **382**, 36 (2013).
20) S. Choi et al., J. Cryst. Growth **388**, 137 (2014).
21) J. Kim et al., J. Cryst. Growth **388**, 143 (2014).
22) M. D. Smith et al., J. Mater. Chem. C **2**, 5787 (2014).
23) E. Taylor, M. D. Smith, T. C. Sadler, K. Lorenz, H. N. Li, E. Alves, P. J. Parbrook, and R. W. Martin, J. Cryst. Growth **388**, 137 (2014).
24) P. Horenburg, E. R. Buß, U. Rossow, H. Bremers, F. A. Ketzer, and A. Hangleiter, Appl. Phys. Lett. **108**, 102105 (2016).
25) S. F. Chichibu, K. Hazu, K. Furusawa, Y. Ishikawa, T. Onuma, T. Ohtomo, H. Ikeda, and K. Fujido, J. Appl. Phys. **116**, 213501 (2014).
26) S. F. Chichibu, K. Kojima, A. Uedono, and Y. Sato, Adv. Mater. **2017**, 29 (2017).
27) J. E. Northrup and J. Neugebauer, Phys. Rev. B **53**, R10477 (1996).
28) C. B. Lim, A. Ajay, and E. Monroy, Appl. Phys. Lett. **111**, 022101 (2017).
29) E. C. H. Kyle, S. W. Kaun, F. Wu, B. Bonef, and J. S. Speck, J. Cryst. Growth **454**, 164 (2016).
30) O. Ambacher, M. S. Brand, R. Dimitrov, T. Metzger, M. Stutzmann, R. A. Fischer, A. Miehr, A. Bergmaier, and G. Dollinger, J. Vac. Sci. Technol. B **14** (1996).
31) H. Yamada, K. Iso, M. Saito, H. Masui, K. Fujito, S. P. DenBaars, and S. Nakamura, Appl. Phys. Express **1**, 041101 (2008).